Equation (III) shows that, because of electromagnetic corrections, the corresponding giant resonance level should have rather smaller energy in negatron decay.

Also in heavier nuclei the collective level as discussed above might have some influence on the relevant nuclear matrix element $\langle ir\rangle$. It is known that the observed $E1$ gamma transitions with small energies have extremely small probabilities in comparison with the shell-model values. Our analysis of RaE shows that the absolute magnitude of $\langle ir\rangle$ cannot be very small. While the $\log ft$ for RaE is 8.0, $\log f_e t \leqq 9.4$.[8] This represents that

$$|\langle ir\rangle| \cong |\langle \boldsymbol{\sigma}\times\mathbf{r}|\rangle| \geqq 0.09R,$$

which is not so much smaller than the shell-model prediction.

PHYSICAL REVIEW VOLUME 126, NUMBER 1 APRIL 1, 1962

Helium-Ion-Induced Fission of Bi, Pb, Tl, and Au†

J. R. HUIZENGA, R. CHAUDHRY,* AND R. VANDENBOSCH
Argonne National Laboratory, Argonne, Illinois

(Received November 20, 1961)

The fission cross sections have been measured with solid-state detectors for helium-ion-induced fission of bismuth, lead-206, thallium, and gold. The measurements were made at several helium-ion projectile energies between 30 and 43 Mev. The fission cross sections of bismuth, lead-206, thallium, and gold with 42.8-Mev helium ions are 7.3, 1.8, 0.65, and 0.28 mb, respectively, and the cross sections decrease rapidly with reduced-energy projectiles. The competition between fission and neutron emission as a function of excitation energy is compared with theoretical predictions of Γ_f/Γ_n and some comments are made on the effect of nuclear deformation on the Fermi gas level density parameter a. Fission thresholds for At^{213}, Po^{210}, $Bi^{207,209}$, and Tl^{201} of 15.8±2.0, 18.6±2.0, 20.6±2.0, and 19.9±2.0 Mev are derived. The saddle-point masses of these nuclei relative to Cameron's reference mass surface lie on a smooth curve with the heavy element data, indicating that the shell structure is completely destroyed during the distortion from equilibrium to saddle-point deformation. An empirical equation for fission thresholds is deduced from the saddle-point mass surface which is thought to be valid for nuclei with Z^2/A between 32 and 40.

I. INTRODUCTION

EXCITATION functions for heavy-element ($Z \geqslant 90$) fission have been measured[1] with a variety of projectiles. In these elements, fission accounts for a major share of the compound nucleus cross section. In addition, the competition between fission and neutron emission is rather independent of excitation energy.[2]

The fission of elements in the vicinity of lead shows quite different characteristics. The fission excitation functions have a strong energy dependence and the fission cross sections reach only a small fraction of the compound nucleus cross section even at excitation energies produced with 40-Mev helium-ion projectiles.

Preliminary measurements of fission excitation functions for target elements with $Z<88$ and at excitation energies less than 50 Mev were first made by Neuzil[3] using radiochemical techniques. Similar measurements were made recently by Nicholson[4] with proportional counters. The counting technique has several advantages over the radiochemical technique. Among the difficulties inherent in the radiochemical fission cross-section measurements are assumptions about the fission fragment mass and charge distributions, incomplete and erroneous decay scheme data, and the problems associated with absolute beta and gamma counting. Direct detection of the fission fragments with solid-state junction counters was employed in this research.

The fission fragment cross sections were measured for helium-ion-induced fission of bismuth, lead-206, thallium, and gold. From the fission cross-section measurements, the competition between fission and neutron emission (or the fission probability) was deduced as a function of the excitation energy. The fission probability is related to the height of the potential barrier which controls the fission process. The barrier arises from the forces involved in the large nuclear distortions which lead to fission. As the nucleus is distorted, the increase in the energy due to the nuclear forces (which act approximately as a surface tension) is initially greater than the decrease in Coulomb energy. However, at some distortion, usually designated as the saddle-point deformation, the decrease in Coulomb energy becomes equal to the increase in surface energy and the nucleus

† Based on work performed under the auspices of the U. S. Atomic Energy Commission.

* On leave from Atomic Energy Establishment, Trombay, India, under sponsorship of the International Cooperation Administration.

[1] References to some of these data can be found in recent review articles on fission (see references 2, 24, and 25).

[2] R. Vandenbosch and J. R. Huizenga, *Proceedings of the Second United Nations International Conference on the Peaceful Uses of Atomic Energy* (United Nations, Geneva, 1958), Vol. 15, p. 284, Paper P688.

[3] E. F. Neuzil, University of Washington, thesis, 1959 (unpublished).

[4] W. J. Nicholson, Jr., University of Washington, thesis, 1960 (unpublished).

becomes unstable to fission. The maximum in the potential energy (ignoring zero-point energy) curve as a function of deformation is defined as the barrier height or fission threshold. As has been pointed out by Swiatecki,[5] the barrier shapes of elements near lead are thought to be considerably simpler than the corresponding barrier shapes for transuranic nuclei and therefore, from a theoretical viewpoint, it is particularly interesting to investigate these barriers. The compound nuclei, At^{213}, Po^{210}, $Bi^{207,209}$, and Tl^{201}, which are investigated in this research are near to closed shells and, hence, their fission thresholds must contain a shell correction energy as well as a "liquid drop" deformation energy. A study of such nuclei may give information on the degree that the shell structure is destroyed at the highly distorted saddle-point deformation.

II. EXPERIMENTAL PROCEDURE

A. General

The helium-ion projectiles were accelerated to a maximum energy of 43 Mev in the Argonne fixed-frequency cyclotron. The energy of the helium-ion projectiles was reduced by foil degradation with an energy degrading-focusing system.[6] In the present experiment the emergent beam is focused, deflected through 30°, degraded, refocused, and passed through a concrete wall into an experimental tunnel. Focusing and deflection coils in the tunnel give control of the beam entering the 11-in. scattering chamber. The collimating system restricts the diameter of the beam at the target to less than $\frac{3}{16}$ in. The helium-ion current on the target varied from 0.05 to 0.3 μa. The total number of helium ions striking the target was measured with a Faraday cup and a vibrating reed electrometer, the output of which was fed to an integrator. The energy of the emergent helium-ion beam was determined by range measurements. The measured mean ranges of the helium ions were converted to energies with the range-energy relationship determined for protons[7] and the assumption that the energy loss of different particles has the same velocity dependence $F(v)$ so that $R=(M/Z^2)F(v)$.

Preliminary measurements[8] indicate that the emergent beam of helium ions has an energy spread with a full width at half-maximum intensity of about 0.4 Mev.

B. Target Preparation

Uniform targets of natural bismuth, lead, thallium, and gold, and, in addition, lead-206 were prepared by volatilization of the element onto 0.0003-in. aluminum backing foils. Several targets of each material with thicknesses ranging from 0.1 to 1 mg/cm^2 were prepared. The elements bismuth and gold are monoisotopic. The lead-206 targets were of the following isotopic composition: Pb^{206} (88%), Pb^{208} (3%), and Pb^{207} (9%).

The purity of all the targets was determined by observing the fission-fragment kinetic-energy spectrum at a reduced helium-ion bombarding energy. Bombarding energies were chosen at which the fission cross sections of the targets were very small and the fission cross section of possible heavy-element contaminants still large. The search for trace amounts of contaminant with $Z>90$ is facilitated by the considerably different fission-fragment kinetic-energy spectra of these elements. A detectable amount of heavy-element fission was not observed for any of the targets.

The target densities (mg/cm^2) were determined by weighing the aluminum backing foils of about 20 cm^2 area before and after the volatilization of the sample. The density of each target for a central portion of the sample was also determined by a colorimetric procedure.

C. Fission Fragment Detectors and Electronics

The solid-state detectors used for the counting and identification of the fission fragment pulses are similar to those described[9] earlier. The sensitive area of the detectors is about 0.3 cm^2 and the calibration[10] of the sensitive area is discussed elsewhere. The detectors were located about 10 cm from the fissionable sample, giving an angular resolution of about 3°. In some of the measurements of the $W(174.5°)/W(90°)$ ratio at the smaller bombarding energies, the detector at 90° was moved to within 4 cm of the target. This gave an angular resolution of about 9°. From angular distribution measurements[11] it can be seen that the fission fragment intensity per unit solid angle is rather constant for angles $90°\pm10°$, and hence the larger solid angle of the 90° detector introduces a negligible error in the $W(174.5°)/W(90°)$ ratio.

The electronic system used in these experiments is similar to that described[9] previously. Measurements were always made at two angles simultaneously. After amplification, the fission pulses from each detector were fed into separate halves of a 256-channel analyzer.

III. EXPERIMENTAL RESULTS

The fission cross sections were calculated from the measured differential fission cross sections. The target bisected the angle between the two detectors in all runs. The laboratory counting rates and angles were converted to the corresponding center-of-mass values with the assumption of full momentum transfer[12] of the

[5] S. Cohen and W. J. Swiatecki, Aarhus Universitet Report, 1961 (unpublished).
[6] W. J. Ramler, J. L. Yntema, and M. Oselka, Nuclear Instr. and Methods **8**, 217 (1960).
[7] H. Bichsel, Phys. Rev. **112**, 1089 (1958); H. Bichsel, R. F. Mozley, and W. A. Aron, *ibid.* **105**, 1788 (1957).
[8] T. Braid (private communication).
[9] R. Vandenbosch, H. Warhanek, and J. R. Huizenga, Phys. Rev. **124**, 846 (1961).
[10] J. R. Huizenga, R. Vandenbosch, and H. Warhanek, Phys. Rev. **124**, 1964 (1961).
[11] R. Chaudhry, R. Vandenbosch, and J. R. Huizenga, following paper [Phys. Rev. **126**, 220 (1962)].
[12] W. J. Nicholson and I. Halpern, Phys. Rev. **116**, 175 (1959).

helium ions to the compound nucleus. The fission fragments were assumed to have kinetic energies[13] equal to an average energy of 70 Mev for the compound nucleus Tl^{201} and 74 Mev for the compound nucleus At^{213}.

The fission cross section with 42.8-Mev helium ions which is calculated with the anisotropy expression derived from the experimental fission fragment angular distribution is about 12% less (see Appendix) than the comparable value deduced with the simple anisotropy expression derived from a two-angle fit, namely, $W(\theta)/W(90°)=1+(b/a)\cos^2\theta$. In the calculation of σ_f at reduced helium-ion energies it has been assumed that the simple anisotropy expression, $W(\theta)/W(90°)=1+(b/a)\cos^2\theta$, gives fission cross sections which are about 12% too large in analogy with the results obtained with 42.8-Mev helium ions.

The fissionable targets were thin enough such that self-absorption of the fission fragments was completely negligible in our counting arrangement. This fact was established by techniques described[10] previously. The number of fission fragment counts in the laboratory system for a fixed helium-ion current was determined by integrating the number of pulses in the fission fragment spectrum as observed with a multichannel analyzer. The valley between the fission fragment pulses and the pulses from the scattered helium ions is illustrated for two helium-ion energies in Fig. 1. At the lower energy where the σ_f has decreased a factor of 500, the valley between the fission fragments and scattered helium ions has increased relative to the height of the fission peak. The helium-ion current on the target was usually kept below 0.2 μa to keep the intensity of the pulses due to pileup of the scattered alpha particles at a tolerable level.

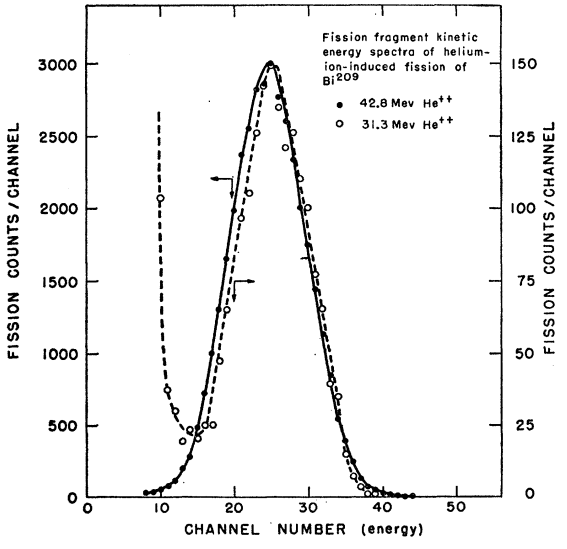

FIG. 1. Fission fragment kinetic energy spectra of helium-ion-induced fission of Bi^{209}. The solid points and open circles were obtained for helium-ion-bombarding energies of 42.8 and 31.3 Mev, respectively.

[13] R. Vandenbosch and J. R. Huizenga (to be published).

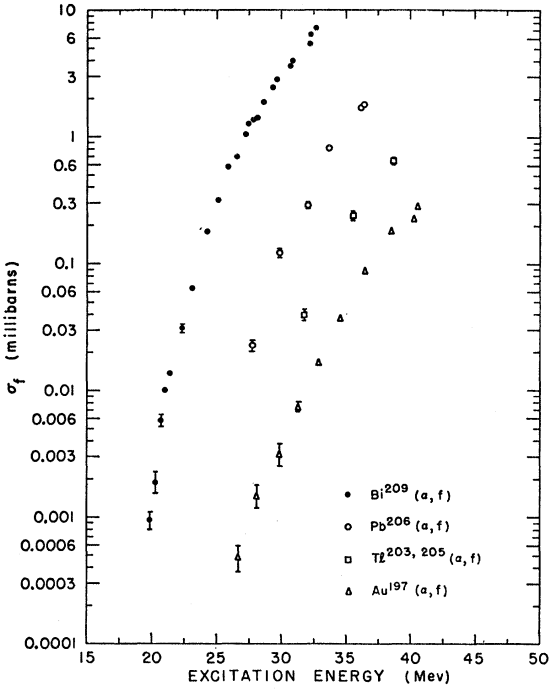

FIG. 2. Fission cross sections for helium-ion-induced fission of bismuth, Pb^{206}, thallium, and gold as a function of the excitation energy of the compound nucleus (assuming full momentum transfer). *Note added in proof.* Due to an error in the target weight of gold, the fission cross sections of gold should be increased by a factor of 1.5. Also see caption in Table II.

The fission cross sections of the targets, Bi^{209}, Pb^{206}, $Tl^{203,205}$ (natural thallium), and Au^{197} bombarded with helium ions of various energies are plotted in Fig. 2. The abscissa in Fig. 2 is given in terms of the excitation energy of the compound nucleus which is formed on absorption of the helium ions. For each target the largest excitation energy represents the maximum helium-ion energy of 42.8 Mev which is obtainable with the Argonne cyclotron. The binding energies of helium ions to targets employed in this study which were used in computing the excitation energies were taken from the compilation of Everling *et al.*[14] The statistical error due to counting is given when it exceeds the physical size of the point which is plotted. The sum of the systematic errors in the fission cross sections due to uncertainties in the target thickness, integrated beam current, detector solid angle, and fission fragment anisotropy is thought to be less than 10% for all targets.

The fission cross sections are calculated and plotted in Fig. 2 on the basis that the helium ions have a monoenergetic energy equal to that of the mean value of the energy distribution. Preliminary measurements[8] indicate that the emergent beam of helium ions (43 Mev)

[14] F. Everling, L. A. König, J. H. E. Mattauch, and A. H. Wapstra, Nuclear Phys. 18, 529 (1960).

has an energy spread with a full-width at half-maximum intensity of about 0.4 Mev. The energy spread of the helium-ion beam at lower energies has been determined by combining the energy spread of the emergent beam with calculated values[15] of the energy spread introduced by the energy loss in the aluminum absorbers. From such a calculation, for example, one obtains a full-width at half-maximum intensity for 30-Mev helium ions (a most probable energy loss of 13 Mev) of 0.5 Mev. Combining this energy spread with the energy spread of the emergent beam gives a full-width at half-maximum intensity of 0.65 Mev for the 30-Mev helium-ion beam. For most of the cross section values in Fig. 2, the error introduced by the assumption of a monoenergetic beam instead of the actual beam with energy spread is less than the statistical error. For example, if one assumes a Gaussian energy distribution of the helium ions with a full-width at half-maximum intensity of 0.65 Mev and an energy dependence of the fission cross section which is linear on a semilog plot and varying a factor of 3 per Mev of energy, the actual fission cross section is 5% smaller than the plotted value. The only values of the fission cross section which may be significantly altered, after corrections for the energy spread in the beam, are the lowest energy values for the Bi^{209} target. The fission cross section is varying at the lowest energies by a factor of 10 per Mev and the actual fission cross sections may be decreased by as much as 25% from the values plotted in Fig. 2.

IV. DISCUSSION

A. Competition Between Fission and Neutron Emission

The fission cross sections presented in Fig. 2 can be used to deduce quantitative information on the ratio of the partial widths for fission and neutron emission. The targets employed in these measurements have high enough Coulomb barriers such that charged particle emission is relatively unimportant and most of the total reaction cross section is accounted for by neutron emission. Excitation functions for (α,xn) reactions have been measured for part of the targets employed in this study. The measurements are incomplete, however, in that at least one of the excitation functions with $x<4$ has not been investigated. Therefore, we have chosen to approximate the neutron emission cross section by the total reaction cross section calculated with an optical model. If one neglects the contribution of fission following neutron emission, Γ_f/Γ_n may be derived from σ_f/σ_R where σ_R is the total reaction cross section taken from the calculations[16] of Huizenga and Igo. The resulting dependence of Γ_f/Γ_n on excitation energy is illustrated by the data which are plotted in Fig. 3.

[15] T. E. Cranshaw, *Progress in Nuclear Physics* (Pergamon Press, Ltd., London, 1952), Vol. 2, p. 271.

[16] J. R. Huizenga and G. J. Igo, Nuclear Phys. **29**, 462 (1962); Argonne National Laboratory Report ANL-6373, 1961 (unpublished).

Although one concludes immediately from the steep slopes of the Γ_f/Γ_n curves that most of the fissions occur before neutron emission, a semiquantitative estimate of second-chance fission can be made in the following way. The average energy carried away by a neutron is the sum of the neutron binding energy and the average neutron kinetic energy. Beginning with the compound nucleus Tl^{201} at a total excitation energy of 40 Mev, one estimates the nuclear temperature of the residual nucleus following neutron emission to be at least 1.2 Mev and hence the average total energy carried off by the neutron to be approximately 10.5 Mev. From Fig. 3 the corresponding values of Γ_f/Γ_n at 40.0 and 29.5 Mev of excitation energy are 1.3×10^{-4} and 2.0×10^{-6}, respectively. From such a calculation one concludes that the contribution of second-chance fission for the initial compound nucleus Tl^{201} excited to 40 Mev is approximately 1.5%. Similar estimates for the other compound nuclei which were investigated suggest that second-chance fission is less than 3% at all of our excitation energies, and hence no corrections were made for it.

It is of interest to compare the experimental values of Γ_f/Γ_n with theoretical predictions in order to deduce information about fission thresholds. The fission width Γ_f has been given by Bohr and Wheeler[17] as

$$\Gamma_f=\frac{1}{2\pi\rho(E')}\int_0^{E-E_f'}\rho^*(E-E_f'-\epsilon)d\epsilon, \qquad (1)$$

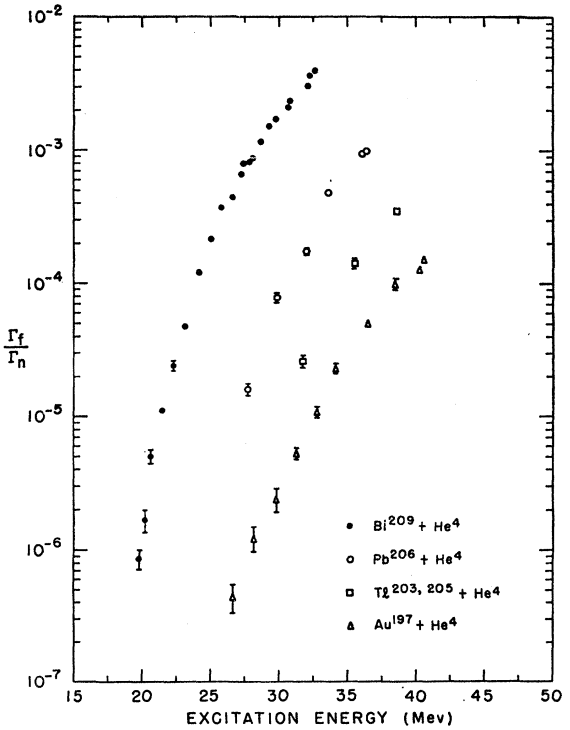

FIG. 3. The fission to neutron emission ratio as a function of excitation energy.

[17] N. Bohr and J. A. Wheeler, Phys. Rev. **56**, 426 (1939).

where $\rho(E')$ is the level density of the excited compound nucleus at the equilibrium deformation, $\rho^*(E-E_f'-\epsilon)$ is the level density of the nucleus at the saddle-point deformation, E is the excitation energy of the compound nucleus, $E'=E-\Delta_s{}^c-\Delta_p{}^c$, and E_f' is the effective fission barrier which is equal to $E_f+\Delta_s{}^f+\Delta_p{}^f$. The terms $\Delta_s{}^c$ and $\Delta_p{}^c$ are the shell and pairing effects at the equilibrium deformation and $\Delta_s{}^f$ and $\Delta_p{}^f$ are similar corrections at the saddle-point deformation. The above expression for the fission width implies that for excitation energies equal to or less than the barrier, $\Gamma_f=0$, since no account is taken of barrier penetration. The neutron width Γ_n has been derived by Weisskopf[18] as

$$\Gamma_n=\hbar\int_0^{E-B_n'} W_n(\epsilon)d\epsilon, \tag{2}$$

where

$$W_n(\epsilon)d\epsilon=\sigma(E,\epsilon)gm\epsilon(1/\pi^2\hbar^3)[\rho(E-B_n'-\epsilon)/\rho(E')]d\epsilon,$$

E is the excitation energy of the compound nucleus, ϵ is the neutron kinetic energy, $\sigma(E,\epsilon)$ is the cross section for the inverse process, g is the statistical weight for the spin states and equal to 2 for neutrons, m is the mass of the neutron, $\rho(E-B_n'-\epsilon)$ is the level density of the residual nucleus and following neutron emission, and $B_n'=B_n+\Delta_s{}^n+\Delta_p{}^n$. The terms $\Delta_s{}^n+\Delta_p{}^n$ are the shell and pairing corrections for the residual nucleus following neutron emission.

A question may be raised about the validity of a statistical model treatment at these high excitation energies where the level width becomes comparable to or greater than the level spacing. The mere overlapping of the levels is not especially troublesome as one can still speak of the average transition probability per unit energy interval. More troublesome is the fact that the lifetimes corresponding to these large widths may become comparable to the time required to transmit information across the nucelus, so that the concept of a compound nucleus with its internal motion randomized among the various degrees of freedom is no longer valid. Insertion of reasonable estimates of the various quantities into Eq. (2) indeed shows that at the highest excitation energies encountered in these experiments the lifetime for neutron emission may be as short as $\sim 10^{-19}$ sec. With this reservation we shall proceed to use the predictions of statistical theory for want of a better procedure.

If one takes for the level density the prediction of the Fermi gas, namely,

$$\rho(E)=\text{const}\exp 2(aE')^{\frac{1}{2}}, \tag{3}$$

and neglects the energy dependence of the pre-exponential constant, one can simplify Eqs. (1) and (2) and derive an expression of the following form:

$$\Gamma_f/\Gamma_n=K_0\frac{a_n}{a_f}\frac{[2a_f{}^{\frac{1}{2}}(E-E_f')^{\frac{1}{2}}-1]}{4A^{\frac{2}{3}}(E-B_n')}\times\exp[2a_f{}^{\frac{1}{2}}(E-E_f')^{\frac{1}{2}}-2a_n{}^{\frac{1}{2}}(E-B_n')^{\frac{1}{2}}], \tag{4}$$

where $K_0=(\hbar^2/gmr_0{}^2)$ is a numerical constant taken as 9.8 Mev, and a_n and a_f are the level density parameters appropriate to the residual nucleus following neutron emission and the fissioning nucleus at the saddle-point deformation.

The choice of the level density parameters a_n and a_f in Eq. (4) is uncertain. Le Couteur and Lang[19] have compiled data on the dependence of a with mass number A deduced from the energy spectra of evaporated particles. They conclude that a is roughly about $A/8$. Near the double closed shell at Pb^{208} the value of a drops sharply for low excitation energies. However, some experimental evidence exists at higher energies[20] which does not show this tendency. Recent analyses of neutron spectra[21] from (p,n) reactions suggest $a\approx A/11$. The targets employed in the present study are rather close to the $Z=82$, $N=126$ closed shells. Comparison of Monte Carlo evaporation calculations[22] with experimental $Bi^{209}(\alpha,xn)$ cross sections gives a lower limit of $a_n=5.3$ Mev^{-1} if shell and pairing effects are neglected. Inclusion of these effects[22] leads to a value of a_n which may be more than twice as large. In the absence of clear indication as to the values of a_n and a_f, we rather arbitrarily tried to fit Eq. (4) with different values of the parameters a_n, a_f, B_n', and E_f'. As has been noted by Nicholson,[4] the magnitudes and energy dependence of the fission to neutron emission ratios, which are plotted in Fig. 3, cannot be reproduced with Eq. (4) if a_n and a_f are kept equal regardless of the value of E_f' chosen. However, by allowing a_n and a_f to take on different values in addition to varying E_f' for a particular value of B_n', it is possible to vary the magnitude and energy dependence of Γ_f/Γ_n as desired. The results of calculations of Γ_f/Γ_n for compound nucleus At^{213} with Eq. (4) in which a_n, a_f, and E_f' are variable parameters are shown in Fig. 4. The calculated results which are plotted in Fig. 4 were based on the assumption that $\Delta_s{}^n=\Delta_p{}^n=0$ and hence $B_n'=B_n$. It became clear from trial and error that it should be possible to fit the experimental curves by some suitable choice of the parameters a_n, a_f, B_n', and E_f'.

For the calculation in which values of a_n and B_n' are assumed as input parameters, Eq. (4) was reduced to the form

$$(kx-1)+\ln(kx-1)=2\ln k+\ln y, \tag{5}$$

[18] V. F. Weisskopf, Phys. Rev. **52**, 295 (1937).

[19] K. J. Le Couteur and D. W. Lang, Nuclear Phys. **13**, 32 (1959).

[20] Data of E. E. Gross, discussed in reference 19.

[21] R. L. Bramblett and F. W. Bonner, Nuclear Phys. **20**, 395 (1960).

[22] R. Vandenbosch, J. R. Huizenga, W. F. Miller, and E. M. Keberle, Nuclear Phys. **25**, 511 (1961).

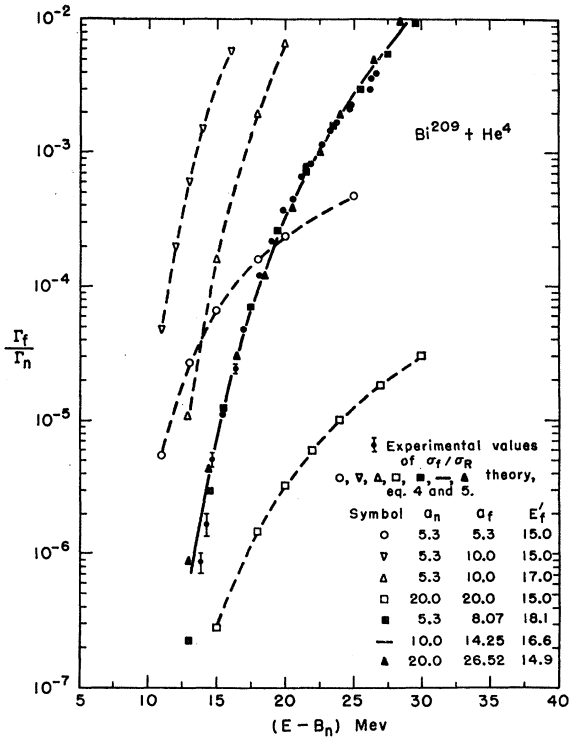

FIG. 4. Theoretical fit of the energy dependence of the fission to neutron emission ratio for helium-ion-induced fission of Bi^{209}. In these calculations B_n' is assumed equal to B_n. The dashed curves were calculated for fixed values of a_n, a_f, and E_f'. The values represented by solid triangles, solid squares, and the solid line were calculated by choosing a value of a_n and determining the values of a_f and E_f' which give the "best fit" to the experimental data.

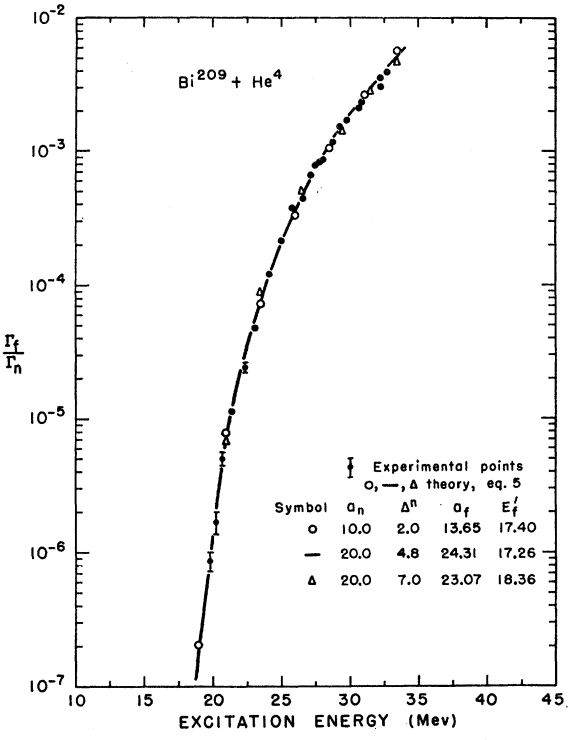

FIG. 5. Theoretical fit of the energy dependence of the fission to neutron emission ratio for helium-ion-induced fission of Bi^{209}. In these calculations $B_n'=B_n+\Delta^n$. For fixed values of a_n and Δ^n, the values of a_f and E_f' were determined which give the "best fit" to the experimental data.

where

$$k=2a_f^{\frac{1}{2}}, \quad x=(E-E_f')^{\frac{1}{2}},$$

and

$$y=(E-B_n')(\Gamma_f/\Gamma_n)(A^{\frac{2}{3}}/a_nK_0)\exp[2a_n^{\frac{1}{2}}(E-B_n')^{\frac{1}{2}}-1].$$

After choosing values of a_n and B_n', Eq. (5) was solved for three values of y, corresponding to three different excitation energies, to get consistent values of k and x at each point. This was accomplished by varying k, until nearly identical values of E_f' were obtained at the three chosen excitation energies. The results for $B_n'=B_n$ and three different choices of a_n, namely, 5.3, 10.0, and 20.0 Mev^{-1} are illustrated in Fig. 4 for the compound nucleus At^{213}.

Neutron emission from the compound nucleus At^{213} gives the residual nucleus At^{212} which is of odd-odd type. Due to the nearness of the double closed shell, the shell correction $\Delta_s{}^n$ for At^{212} is appreciable (the ground-state mass is depressed relative to Cameron's[23] reference mass by approximately 4 Mev). Some of the results of calculations of Γ_f/Γ_n for the compound nucleus At^{213} with Eq. (4) in which $\Delta_p{}^n+\Delta_s{}^n$ is varied from 2 to 7 Mev are given in Fig. 5. In these calculations, the level density in the residual nucleus following neutron emission is initiated $(\Delta_p{}^n+\Delta_s{}^n)$ Mev in excess of the ground-state mass. As can be seen from the agreement of experimental and calculated values of Γ_f/Γ_n in Figs. 4 and 5, it is possible to reproduce the experimental data with widely different values of B_n' and a_n.

Similar calculations were made for all the other targets for various choices of a_n and B_n'. For some of the calculations, shell and pairing corrections of the order of magnitude of those of Cameron[23] were chosen for the residual nucleus following neutron emission. The "best fit" values of a_f and E_f' for all the compound nuclei are summarized in Table I.

For the calculation in which a_f and B_n' are assumed as input parameters, Eq. (4) was reduced to the form,

$$(cx-1)+\ln(cx-1)=(kn-1)-2\ln k+\ln y, \quad (6)$$

where

$$k=2a_n^{\frac{1}{2}}, \quad x=(E-E_f'-E_R{}^f)^{\frac{1}{2}}, \quad n=(E-B_n'-E_R)^{\frac{1}{2}},$$

$$C=2a_f^{\frac{1}{2}}, \text{ and } \quad y=(16a_fA^{\frac{2}{3}}/K_0)(E-B_n'-E_R)(\Gamma_f/\Gamma_n).$$

In these calculations a_f has been assumed[19] equal to $A/8$. The choice of the magnitude of $\Delta_p{}^n+\Delta_s{}^n$ was influenced by the following considerations. Previous calculations had shown that in order to get reasonable agreement between the calculated and experimental values of

[23] A. G. W. Cameron, Atomic Energy of Canada Limited Report CRP-690, 1957 (unpublished).

TABLE I. "Best fit" values of a_f values and E_f' deduced from the fission to neutron emission competition for selected values of a_n and B_n' as described in the text, where $B_n'=B_n+\Delta_s{}^n+\Delta_p{}^n$. A positive delta value in this table means that the ground-state mass is less than the reference mass from which the level density is initiated.

Target	a_n (Mev^{-1})	$(\Delta_s{}^n+\Delta_p{}^n)$ (Mev)	a_f (Mev^{-1})	E_f' (Mev)
Au^{197}	5.3	0	6.71	24.41
	10.0	0	12.39	22.09
	20.0	0	23.81	19.52
	20.0	3	23.04	21.17
$Tl^{203,205}$ (natural)	10.0	0	13.23	21.29
	20.0	0	24.87	18.79
	20.0	7.7	22.95	23.21
Pb^{206} (88%)	10.0	0	13.76	20.14
	20.0	0	25.65	17.96
	20.0	7.7	23.22	22.17
Bi^{209}	5.3	0	8.07	18.08
	10.0	0	14.25	16.61
	10.0	2	13.65	17.40
	20.0	0	26.52	14.91
	20.0	4.8	24.31	17.26
	20.0	7.0	23.07	18.36

Γ_f/Γ_n as a function of energy, a_f must be larger than a_n. This can be reasonably well understood by noting that at the saddle-point deformation the shell structure associated with the spherical shape has been destroyed and the level density parameter a_f should resemble the value expected for deformed nuclei of the same mass in regions far from closed shells. For nuclei near closed shells the level density parameter a_n is reduced and its magnitude is expected to be related to the size of the shell correction and the excitation energy. At very high excitation energies the shell structure is destroyed and a_n is expected to approach a_f. In treating our experimental data with Eq. (6), the value of a_n is assumed to be constant over several Mev of energy. Although this is not expected to be true, the calculations of the fission thresholds are rather insensitive to small changes in a_n.

TABLE II. "Best fit" values of a_n and E_f' deduced from the fission to neutron emission competition for $a_f=A/8$ and selected values of B_n', where $B_n'=B_n+\Delta_s{}^n+\Delta_p{}^n$. The appropriate rotational energies were included in these calculations as discussed in the text. A positive delta value in this table means that the ground-state mass is less than the reference mass from which the level density is initiated. *Note added in proof.* Increasing the fission cross sections of gold by a factor of 1.5 produces a very small change in a_n and E_f'. With the corrected values of Γ_f/Γ_n for gold, the "best fit" values of a_n and E_f' are 21.63 Mev^{-1} and 19.83 Mev, respectively.

Target	a_f (Mev^{-1})	$(\Delta_s{}^n+\Delta_p{}^n)$ (Mev)	a_n (Mev^{-1})	E_f' (Mev)
Au^{197}	25.12	1.5	21.94	19.90
$Tl^{203,205}$ (natural)	26.00	3.85	22.23	20.57
Pb^{206} (88%)	26.25	3.85	21.90	19.73
Bi^{209}	26.62	2.4	21.44	15.81
	26.62	4.8	22.66	16.95

In most of our calculations the excitation energies of the residual nuclei following neutron emission are of the order of 20 Mev. It seems reasonable, therefore, that the absolute value of $\Delta_s{}^n$ appropriate in each calculation should be reduced from the value calculated from the ground-state[14] mass and Cameron's reference mass. That is to say, the absolute magnitudes of the shell correction for nuclei in the vicinity of lead are expected to decrease with increasing excitation energy.

The level density reference surface has been chosen as equal to the odd-A surface adjusted for a shell correction (which is excitation energy dependent). Values of $\Delta_s{}^n$ ranging from 0.4 to 0.6 of the corresponding ground-state shell corrections were finally chosen in the final calculations. In the case of the Bi^{209} target, a calculation was also made with $\Delta_s{}^n+\Delta_p{}^n=4.8$ Mev. The "best fit" values of a_n and E_f' which were derived for the four compound nuclei are summarized in Table II. The good agreements between the experimental and calculated values of Γ_f/Γ_n derived from Eq. (6) are shown in Fig. 6.

The rotational energies at the equilibrium and saddle-point deformations are included[24,25] in Eq. (6). The

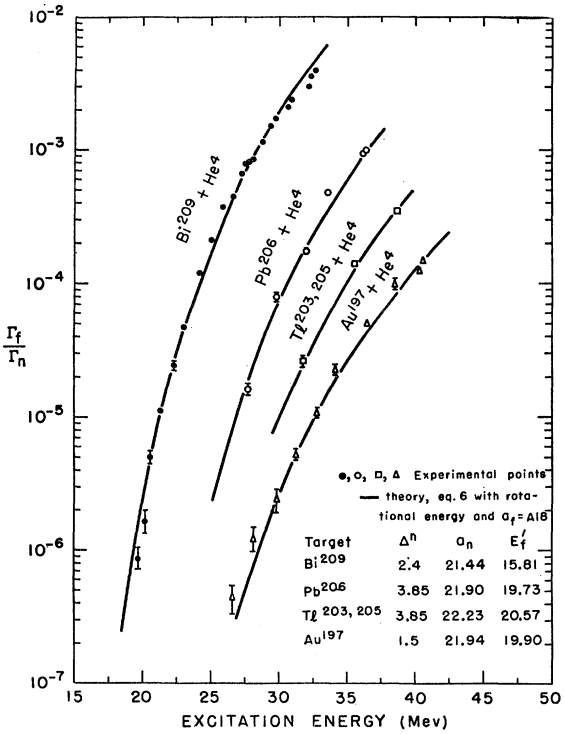

FIG. 6. Theoretical fits of the energy dependence of the fission to neutron emission ratio for helium-ion-induced fission of gold, thalium, Pb^{206}, and bismuth. In these calculations a_f is assumed equal to $A/8$ and Δ^n is about 50% of Cameron's shell correction. Values of a_n and E_f' are determined which give the "best fit" to the experimental data.

[24] I. Halpern, Ann. Rev. Nuclear Sci. 9, 245 (1959).

[25] J. R. Huizenga and R. Vandenbosch, in *Nuclear Reactions*, edited by P. M. Endt and M. Demeur [North-Holland Publishing Company, Amsterdam (to be published)].

value of E_R was assumed equal to $\hbar^2\langle I^2\rangle_{\rm av}/2\mathcal{J}$, where $\mathcal{J}$ is the rigid-body moment of inertia, and $E_R{}^f$ was assumed equal to $0.6\,E_R$. The inclusion of the angular momentum effect in the latter calculations does not change the "best fit" values of a_n and E_f' significantly. This statement must be qualified if calculations of Γ_f/Γ_n are made at excitation energies near the fission threshold. In fact, at low excitation energies if $E_f'\gg B_n'$, Γ_f/Γ_n may even decrease with increasing angular momentum.

An attempt has also been made to fit the experimental data with a level density expression

$$\rho(E)=\text{const}\,\exp(E/T), \qquad (7)$$

where T is taken independent of excitation energy. Using Eq. (13) of reference 25 for the energy dependence of Γ_f/Γ_n for the constant temperature model, the values of Γ_f/Γ_n were calculated for At^{213} and Tl^{201} for a choice of $T_n=1.6$ Mev and plotted as dashed lines in Fig. 7. The "best fits" for the level density law of Eq. (3) are also shown. In this comparison, B_n' was assumed equal to B_n for both equations, although similar results are obtained when the shell and pairing effects are different from zero. The constant-temperature model predicts a dependence of Γ_f/Γ_n at high excitation energies which is a straight line on the semilog representation of Fig. 7. The constant-temperature formulation of the level density does not give quite as good an account of the experimental data as the Fermi gas level density (solid curve) and will not be considered further.

The best estimates of E_f' values are thought to be those in Table II in which $a_f=A/8$ and the values of $\Delta_s{}^n$ are approximately 50% of the ground-state shell correction. The values of E_f' for Tl^{201}, $Bi^{207,209}$, Po^{210}, and At^{213} are then 19.9, 20.6, 19.7, and 15.8 Mev, respectively. If one assigns an error of ± 2 Mev on these values, the limits would include most of the other values of E_f' derived with widely different values of a_n, a_f, and B_n' (see also Table I).

The value of E_f' was defined previously as equal to $E_f+\Delta_s{}^f+\Delta_p{}^f$, where the latter two terms are the shell and pairing corrections at the saddle deformation. In the present experiments E_f is the energy which must be supplied to a ground-state nucleus to reach the lowest energy threshold (e.g., spontaneous fission threshold), whereas E_f' is the energy which must be supplied to a ground-state nucleus to reach the point at which the saddle-point level density is initiated [see Eq. (1)]. For a nucleus in which the fission threshold is larger than the neutron binding energy, E_f' is essentially equivalent to the photofission threshold, since at this energy the photofission to photoneutron emission cross-section ratio would exhibit a marked change in slope. It is assumed that $\Delta_s{}^f=0$, since it is reasonable to believe that at the highly deformed saddle configuration the shell structure has been completely destroyed. The pairing correction at the saddle deformation may be larger[26,27] than the equilibrium pairing correction by about 0.4 Mev, i.e., $\Delta_p{}^f=\Delta_p{}^c+0.4$, although the uncertainty in $\Delta_p{}^f$ is rather large. In evaluating the values of E_f we have rather arbitrarily assumed the saddle-point level density to be initiated from the odd-A mass surface of the highly deformed nucleus. The resulting values of E_f for Tl^{201}, $Bi^{207,209}$, Po^{210}, and At^{213} are 19.9, 20.6, 18.6, and 15.8 Mev, respectively.

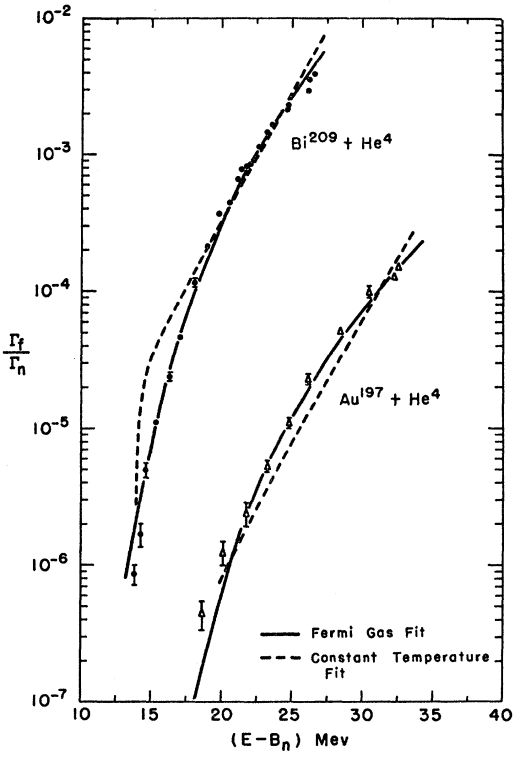

FIG. 7. Comparison of the theoretical fits of the energy dependence of the fission to neutron emission ratio for helium-ion-induced fission of gold and bismuth with the Fermi gas model and a constant-temperature model.

The ground states of the above compound nuclei are unusually stable (as revealed for example by their large shell corrections). The measured fission thresholds, therefore, reflect the extra energy required to break up the ground-state shell structure. In the lower part of Fig. 8, the energy differences between the $(M-A)$ values of Everling *et al.*,[14] which represent the ground-state masses, and the $(M-A)$ values of Cameron's reference mass formula [Eq. (7) in reference 23] are plotted as a function of Z^2/A. The latter parameter has, of course, no significance in such a plot. Heavy element (uranium region) values of this mass difference are also included in Fig. 8. It can immediately be seen from Fig. 8 that the nuclei Tl^{201}, $Bi^{207,209}$, Po^{210}, and At^{213} have ground states which are very much depressed relative to Cameron's reference surface.

Each saddle-point mass $(M-A)_{\rm saddle}$ is calculated by adding the experimental fission threshold E_f and the ground-state mass of Everling *et al.*[14]

[26] W. J. Swiatecki, Phys. Rev. **101**, 97 (1956).
[27] P. Fong, Phys. Rev. **122**, 1545 (1961).

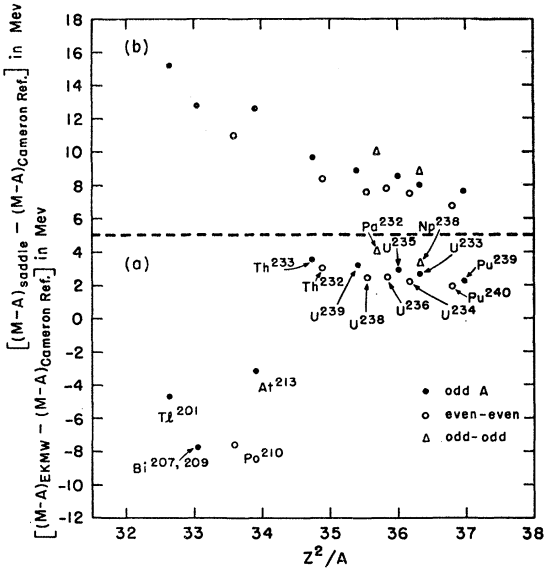

FIG. 8. Ground-state and saddle-shape mass surfaces. (a) The energy differences between the ground-state masses of Everling, König, Mattauch, and Wapstra and the reference masses of Cameron. (b) The energy differences between the masses of the saddle-shape configuration and the reference masses of Cameron.

$(M-A)_{\text{EKMW}}$. The differences between $(M-A)_{\text{saddle}}$ and $(M-A)_{\text{Cameron ref.}}$ are plotted as a function of Z^2/A in the upper part of Fig. 8. Whereas the ground-state masses show a large discontinuity between the two groups of nuclei due to the large shell correction, the saddle-point masses plotted relative to Cameron's reference mass surface lie on a rather smooth curve. This is a rather striking demonstration that the shell structure is completely destroyed when going from the equilibrium to the saddle-point deformation.

The saddle-point masses relative to Cameron's reference surface mass have been corrected for pairing energies to the odd-A mass surface and the resulting values plotted in Fig. 9 as a function of Z^2/A. We have assumed the even-even and odd-odd saddle-point mass surfaces to lie 1.1 Mev below and above the odd-A mass surface, respectively. All of the points in Fig. 9 lie on a smooth line. The saddle-point masses corrected for pairing effects in Fig. 9 are reasonably well represented by the equation: $2370-189.58(Z^2/A)+5.0937(Z^2/A)^2-0.045833(Z^2/A)^3$. The fission thresholds are then given by the empirical equation

$$E_f\ (\text{Mev})=2370-189.58(Z^2/A)+5.0937(Z^2/A)^2-0.045833(Z^2/A)^3-\delta M+\begin{Bmatrix}+1.1\\0\\-1.1\end{Bmatrix}\begin{Bmatrix}\text{o-o}\\\text{odd } A\\\text{e-e}\end{Bmatrix}, \quad (8)$$

where $\delta M=(M-A)_{\text{EKMW}}-(M-A)_{\text{Cameron ref.}}$ is in energy units of Mev. Values of the fission thresholds E_f for nuclei with Z^2/A between 32 and 40 should be reasonably well approximated with Eq. (8).

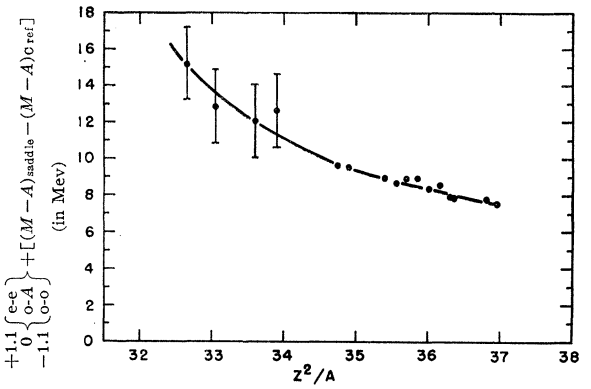

FIG. 9. Saddle-shape masses (relative to Cameron's reference masses) corrected for pairing effects. The amounts of +1.1, 0, and −1.1 Mev are added to the even-even, odd-A, and odd-odd nuclei, respectively.

B. Comparisons with the Liquid Drop Model

The fission thresholds deduced in a previous section may be compared with the liquid drop model calculations of Cohen and Swiatecki.[5] In order to make any such comparison meaningful, the experimental thresholds have to be reduced to correct for the energy which is needed to destroy the shell structure during the deformation to the saddle configuration. If one rather arbitrarily chooses the mass of the liquid drop to be that of Cameron's reference mass, the resulting fission thresholds are considerably smaller than the values calculated by Cohen and Swiatecki.[5]

ACKNOWLEDGMENTS

The authors wish to acknowledge members of the cyclotron group for operation of the cyclotron, W. Bentley for assistance with the electronic equipment, and Miss M. Petheram for reduction of the data. One of us (R. Chaudhry) wishes to thank the International Cooperation Administration, Washington, the International Institute of Nuclear Science and Engineering of the Argonne National Laboratory, and U. S. Atomic Energy Commission for providing opportunity to work at the Argonne National Laboratory.

APPENDIX

If the angular distribution of fission fragments is expressed by

$$W(\theta)=a+b_2\cos^2\theta+b_4\cos^4\theta+b_6\cos^6\theta+b_8\cos^8\theta+b_{10}\cos^{10}\theta, \quad (A1)$$

it is easy to show that

$$\sigma_f=k_1a_0\left(1+\frac{1}{3}\frac{b_2}{a}+\frac{1}{5}\frac{b_4}{a}+\frac{1}{7}\frac{b_6}{a}+\frac{1}{9}\frac{b_8}{a}+\frac{1}{11}\frac{b_{10}}{a}\right), \quad (A2)$$

where k_1 depends on the solid angle of the detectors, the target thickness, and the number of helium-ion projectiles. Measurements at only 0° (or 180°) and 90° can-

not give all the b coefficients in expression (A1). An angular distribution of the form

$$W(\theta)=a+b\cos^2\theta \tag{A3}$$

gives a cross section

$$\sigma_{f1}=k_1 a(1+\tfrac{1}{3}b/a). \tag{A4}$$

From expressions (A2) and (A4), one can write

$$\frac{\sigma_{f1}-\sigma_f}{\sigma_{f1}}=\left[a\left(1+\frac{1}{3}\frac{b}{a}\right)-a_0\left(1+\frac{1}{3}\frac{b_2}{a}+\frac{1}{5}\frac{b_4}{a}+\cdots+\frac{1}{11}\frac{b_{10}}{a}\right)\right]\Big/ a\left(1+\frac{1}{3}\frac{b}{a}\right). \tag{A5}$$

Since the coefficients a and b in Eq. (A3) are obtained by actual measurements at 0° and 90°, one gets $W(90°)=a=a_0$ and

$$W(0°)=a+b=a_0+b_2+b_4+\cdots+b_{10}. \tag{A6}$$

Therefore, Eq. (A5) gives

$$\frac{\sigma_{f1}-\sigma_f}{\sigma_{f1}}=\frac{0.1333b_4/a+0.1904b_6/a+0.2222b_8/a+0.2424b_{10}/a}{1+0.3333b/a}=y. \tag{A7}$$

Thus $\sigma_f=(1-y)\sigma_{f1}$. The angular distribution at 42.8-Mev alpha bombarding energy[11] for a Au^{197} target fitted with terms up to $\cos^6\theta$ gave $b/a=1.5430$, $b_2/a=0.2676$, $b_4/a=0.7282$, and $b_6/a=0.5472$. Thus $y=0.1329$. Therefore, the cross sections obtained by measurement of the angular distribution at only 0° and 90° would be 13% higher.

The angular distribution at 42.8-Mev alpha bombarding energy[11] for a Bi^{209} target fitted with terms up to $\cos^{10}\theta$ gave $b/a=1.2815$, $b_2/a=-0.3792$, $b_4/a=5.6538$, $b_6/a=-11.5362$, $b_8/a=10.5018$, and $b_{10}/a=-2.9587$. Therefore $y=0.12$ and the cross sections measured from angular distributions at only 0° and 90° would be 12% higher.